DINAME 2019 - Proceedings of the XV International Symposium on Dynamic Problems of Mechanics,
M.A. Savi, T.G. Ritto and W.M. Bessa (Editors), ABCM, Buzios, RJ, Brazil, March 10th to 15th, 2019

Nonlinear Dynamical Analysis of a 2-DOF SMA Oscillator Using a Model with Internal Constraints

Daniel .M.B. Netto[1], Pedro M.C.L. Pacheco[1], Alberto Paiva[2] and Marcelo A. Savi[3]

[1] Centro Federal de Educação Celso Suckow da Fonseca – CEFET/RJ – Mechanical Engineering Graduate Program
229 Maracanã Av. – Rio de Janeiro – RJ – Brazil – 27271-110
daniel.netto@aluno.cefet-rj.com, calas@cefet-rj.br

[2] Universidade Federal Fluminense – Volta Redonda School of Engineering – Department of Mechanical Engineering
420 Trabalhadores Av. – Volta Redonda − RJ – Brazil – 27.255-125
albertopaiva@id.uff.br

[3] Universidade Federal do Rio de Janeiro – COPPE – Department of Mechanical Engineering
Center for Nonlinear Mechanics – MECANON – Rio de Janeiro – RJ – Brazil – 21.941.972
savi@mecanica.ufrj.br

*Abstract: A dynamical system with two degrees-of-freedom and three Shape Memory Alloy (**SMA**) restoring elements is proposed. The **SMA** may present a complex behavior due to the solid state-phase transformations involving austenite and martensite, which result in a hysteretic behavior as a consequence of the intrinsic damping and switching properties between both phases. Equations of motion are formulated by assuming a constitutive model with internal constraints. Mathematically, this formulation is highly nonlinear and the responses of the system might be periodic, quasi-periodic, chaotic or even hyperchaotic, as will be addressed in this paper.*

Keywords: Shape memory alloy, constitutive model, internal constraints, nonlinear dynamics.

INTRODUCTION

Shape Memory Alloy (**SMA**) systems and structures applications have become popularized in the last two decades, not only due to **SMA**'s outstanding capacity to develop and recover high strain levels (or to develop huge restoring forces, while constraining their displacement) but also because of their intrinsic damping capacity, both deriving from hysteretic reversible phase transformations.

There are plentiful works involving **SMA** dynamical applications considering different constitutive models, for instance: Bernardini & Rega (2005) numerically evaluate the influence of the change in temperature of the **SMA** restoring element, using their own constitutive model, over a one-degree of freedom oscillator dynamics, as a consequence of the lack of time for heat exchange with the surrounding environment in high-frequency applications; Enemark et al. (2014) performed a numerical-experimental study as well, where the numerical results encompass the constitutive model proposed by Brinson (1993). Sitnikova et al. (2012) carried out a comparison between numerical and experimental results for a 1-**DOF** nonsmooth oscillator, considering an **SMA** discontinuous support. The authors use the same constitutive model of Bernardini & Rega (2005). Gaikwad & Pandey (2018) also use Bernardini & Rega (2005) model in a 1-**DOF SMA** oscillator, considering convection with the surrounding environment.

Many works in the literature employ the polynomial model proposed by Falk (1980); nevertheless, this model has two important limitations: it does not consider any dissipation and does not consider the twinned martensite variant at low temperatures. Among the works using this polynomial model, it is worth to mention: Wang & Melnik (2012) evaluate the performance of a tuned vibration absorber embedded with **SMA**; Rusineka et al. (2017) performed a dynamical investigation of a reconstructed middle ear with a shape memory alloy prosthesis. It is considered a two-degree of freedom model under different external excitation; Rodrigues et al. (2017) study the dynamical stability of the natural response of a two-degree of freedom oscillator, considering different temperatures; and Rajagopal et al. (2018) investigate the system behavior of a two-degree of freedom using bifurcation diagrams for different configurations of temperature at the restoring elements. The physical dynamical model used in the latest three works the same considered in this paper.

Savi and co-workers applied the same constitutive model with internal constraints used herein (Paiva et al. 2005) in different mechanical archetypes for several purposes, for instance, in the upcoming references. It is important to highlight that this model overcomes the limitations assigned above for the Falk polynomial model. Savi et al. (2011) conducted a numerical study, considering an adaptive vibration absorber using **SMA**, based upon resonant dynamical jumps. Savi et al. (2008) investigated the tensile-compressive asymmetry influence over a 1-**DOF SMA** oscillator. Silva et al. (2013) presented a nonlinear analysis of a 2-**DOF** Jeffcott rotor system, undergoing impact between the rotor and the stator, with **SMA** restoring elements on the stator supporting bearings. Aguiar et al. (2013) performed a numerical-experimental analysis of a tuned vibration absorber embedded with **SMA.** Savi (2015) provides a review of dynamical applications involving **SMA** systems, highlighting the use of different constitutive models to describe the shape memory thermomechanical behavior.

This paper deals with the dynamical analysis through numerical simulations of a 2-**DOF** oscillator considering three **SMA** restoring elements. The constitutive behavior of the **SMA** elements is described by an internal constraints model proposed by Paiva et al. (2005). The resulting set of ordinary differential equations is solved using the 4th-order Runge-Kutta method. The preliminary results presented here involve equilibrium points' analysis during free vibration response at low **SMA** temperatures, recalling that many works in the literature only address the pseudoelastic behavior due to constitutive model limitations. Besides that, the forced response is investigated through bifurcation diagrams varying the forcing parameters.

MATHEMATICAL MODELING

This section comprises the mathematical formulation of the coupled constitutive-dynamical model. It is divided in two sections, the first presents the constitutive modelling and the second integrates the constitutive model into the physical model. The set of ordinary differential equations of motion are expressed in dimensionless form to optimize the numerical implementation.

Constitutive Modeling

The constitutive model used to describe the **SMA** behavior is the one-dimensional version of the model proposed by Savi and co-workers (Paiva *et al.* 2005), which is based on the constitutive model with internal constraints (Fremond, 1987). Here, the effects of plasticity and asymmetry between tension-compression are discarded. The model considers four internal variables β_1, β_2, β_3 and β_4 related to tractive detwinned martensite, compressive detwinned martensite, austenite and twinned martensite, respectively. It is possible to express one of the internal state variables (here, twinned martensite is chosen) as a function of the other three, by the relation: $\beta_4 = 1 - \beta_1 - \beta_2 - \beta_3$. Equations (1–4) summarize the set of constitutive equations, where Eq. (1) is the stress-strain-temperature relation, while Eqs. (2–4) provide the internal variables evolution equations.

$$\sigma = E\varepsilon + (\alpha E - \alpha_h)(\beta_2 - \beta_1) + \Theta(T - T_0) \tag{1}$$

$$\dot{\beta}_1 = \frac{1}{\eta_M}\left\{\alpha\varepsilon + \Lambda_M + (2\alpha_h\alpha + E\alpha_h^2)(\beta_2 - \beta_1) + \alpha_h\left[E\varepsilon - \Theta(T - T_0)\right] - \partial_{\beta_1} J_\pi\right\} - \partial_{\dot{\beta}_1} J_\chi \tag{2}$$

$$\dot{\beta}_2 = \frac{1}{\eta_M}\left\{-\alpha\varepsilon + \Lambda_M - (2\alpha_h\alpha + E\alpha_h^2)(\beta_2 - \beta_1) - \alpha_h\left[E\varepsilon - \Theta(T - T_0)\right] - \partial_{\beta_2} J_\pi\right\} - \partial_{\dot{\beta}_2} J_\chi \tag{3}$$

$$\dot{\beta}_3 = \frac{1}{\eta_A}\left\{-\frac{1}{2}(E_A - E_M)\left[\varepsilon + \alpha_h(\beta_2 - \beta_1)\right]^2 + \Lambda_A + (\Theta_A - \Theta_M)(T - T_0)\left[\varepsilon - \alpha_h(\beta_2 - \beta_1)\right] - \partial_{\beta_3} J_\pi\right\} - \partial_{\dot{\beta}_3} J_\chi \tag{4}$$

In these equations, $E = E_M + \beta_3(E_A - E_M)$ is the elastic modulus, $\Theta = \Theta_M + \beta_3(\Theta_A - \Theta_M)$ is coefficient of thermal expansion and T_0 is a reference temperature. The subscript indices "*M*" and "*A*" the parameter α is related to the height of the hysteresis loop, while α_h is related to its width, consequently the residual strain. The term ∂_{β_i} are sub-differentials of the indicator function J_π with respect to the volumetric fraction, β_i (i=1,2,3) relating the internal constrains to the coexistence of phases. The term $\partial_{\dot{\beta}_i}$ are subdifferentials of the indicator function J_χ with respect to β_i (i=1,2,3), which is associated with the proper conditions to describe the internal sub-loops due to the incomplete phase transformations. The dissipation parameters η may assume different values for loading and unloading. The parameters Λ are associated with the critical stress for phase transformations, which are defined as:

$$\Lambda = \begin{cases} -L_0 + \dfrac{L}{T_M}(T - T_M) \text{ if } T > T_M \\ -L_0 \text{ if } T \le T_M \end{cases} \tag{5}$$

$$\Lambda_A = \begin{cases} -L_0^A + \dfrac{L^A}{T_M}(T - T_M) \text{ if } T > T_M \\ -L_0^A \text{ if } T \le T_M \end{cases} \tag{6}$$

where T_M is the critic temperature which martensic phase is stable. The parameters L_0, L, L_0^A e L^A control the phase transformations.

Constitutive-Dynamical Coupled Modeling

Figure 1 presents the physical model for a 2-**DOF** oscillator incorporated of three **SMA** restoring elements. The inertial elements *m* are identical lumped masses with displacement along *x* direction, respectively expressed by $u_1(t)$ and $u_2(t)$; *c* is the damping coefficients, which is considered the same for the three damping elements; besides, an external harmonic forces *F(t)* is imposed on the mass *m*, between **SMA** element #1 and **SMA** element #2.

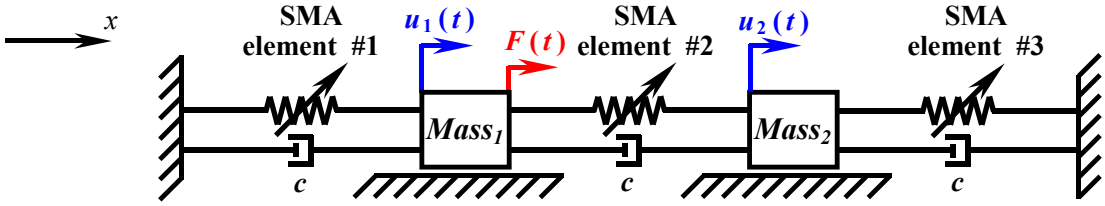

Figure 1 – Physical model.

Newton's equations of motion for the masses are given as follows:

$$\begin{cases} m\ddot{u}_1 = F(t) - F_{R_1} - F_{D_1} + F_{R_2} + F_{D_2} \\ m\ddot{u}_2 = -F_{R_2} - F_{D_2} - F_{R_3} - F_{D_3} \end{cases} \tag{7}$$

The **SMA** restoring elements are assumed as bars, whose force F_{R_i} (for i=1,2,3) is given by: $F_{R_i} = \sigma_i A$, where σ is given by Eq. (1) and A represents the cross-sectional area of the **SMA** bar and L its length. Besides the hysteretic dissipation found on **SMA** solid state-phase transformations, an extra linear viscous dissipation is considered as, $F_D = c\dot{u}$. In equation (8) the two equations of motion are developed based on equation (7) taking account the considerations made.

$$\begin{cases} m\ddot{u}_1 = F\cos(\Omega t) - c\dot{u}_1 + c(\dot{u}_2 - \dot{u}_1) - \left[E\dfrac{u_1}{L} + (\alpha + E\alpha_h)(\beta_{2_1} - \beta_{1_1}) - \Theta(T_1 - T_0)\right]A \\ + \left[E\dfrac{(u_2 - u_1)}{L} + (\alpha + E\alpha_h)(\beta_{2_2} - \beta_{1_2}) - \Theta(T_2 - T_0)\right]A \\ m\ddot{u}_2 = -c\dot{u}_2 - c(\dot{u}_2 - \dot{u}_1) - \left[E\dfrac{(u_2 - u_1)}{L} + (\alpha + E\alpha_h)(\beta_{2_2} - \beta_{1_2}) - \Theta(T_2 - T_0)\right]A \\ - \left[E\dfrac{u_2}{L} + (\alpha + E\alpha_h)(\beta_{2_3} - \beta_{1_3}) - \Theta(T_3 - T_0)\right]A \end{cases} \tag{8}$$

The uniaxial strain **SMA** of the restoring elements are assumed under infinitesimal strain, so the instantaneous uniaxial strain may be considered:

Considering the new variables to express the dimensionless differential equations of motion: $\tau = t\omega$ is the new independent variable, where ω is the angular frequency adopted regarding a reference value, given by: $\omega = \sqrt{E_M A/mL}$; $U = u/L$ is the dimensionless displacement; and $\theta = T/T_M$ is the dimensionless temperature. The derivatives of displacement are replaced by the derivative of the new dimensionless variable $U(\tau)$, which are, $U'(\tau)$ and $U''(\tau)$ where $U'(\tau(t))$, by applying the chain's rule.

$$\frac{dU}{dt} = \frac{\partial U}{\partial \tau}\frac{\partial \tau}{\partial t} = U'\omega \tag{9}$$

$$\frac{d^2U}{dt^2} = \frac{\partial^2 U}{\partial \tau^2}\left(\frac{\partial \tau}{\partial t}\right)^2 = U''\omega^2 \tag{10}$$

The set of dimensionless equations of motion is:

$$\begin{cases} U_1'' = \delta\cos(t\varpi) - \xi U_1' + \xi(U_2' - U_1') - \left[\gamma_1 U_1 + (\overline{\alpha} + \gamma_1\alpha_h)(\beta_{2_1} - \beta_{1_1}) - \overline{\Theta}_1(\theta_1 - \theta_0)\right] \\ + \left[\gamma_2(U_2 - U_1) + (\overline{\alpha} + \gamma_2\alpha_h)(\beta_{2_2} - \beta_{1_2}) - \overline{\Theta}_2(\theta_2 - \theta_0)\right] \\ U_2'' = -\xi U_2' - \xi(U_2' - U_1') - \left[\gamma_2(U_2 - U_1) + (\overline{\alpha} + \gamma_2\alpha_h)(\beta_{2_2} - \beta_{1_2}) - \overline{\Theta}_2(\theta_2 - \theta_0)\right] \\ - \left[\gamma_3 U_2 + (\overline{\alpha} + \gamma_3\alpha_h)(\beta_{2_3} - \beta_{1_3}) - \overline{\Theta}_3(\theta_3 - \theta_0)\right] \end{cases} \tag{11}$$

Regarding the dimensionless parameters of Eq. (11) which replace the original dimension parameter:

$$\xi = \frac{c}{m\omega};\ \gamma = \frac{EA}{mL\omega^2} = \frac{E}{E_M};\ \overline{\alpha} = \frac{\alpha A}{mL\omega^2} = \frac{\alpha\gamma}{E} = \frac{\alpha}{E};\ \overline{\Theta} = \frac{\Theta A T_0}{mL\omega^2} = \frac{\Theta T_M}{E_M};\ \theta_0 = \frac{T_0}{T_M};\ \varpi = \frac{\Omega}{\omega};\ \delta\frac{F}{mL\omega^2} = \frac{F}{E_M A}; \tag{12}$$

The parameters ξ, δ and ϖ are defined directly. The constitutive parameters, $\overline{\alpha}$ and θ_0 are calculated directly from the constitutive model parameters, while γ and $\overline{\Theta}$ respectively depend upon the parameters E and Θ should be recalculated in every step.

Pertaining to the numerical implementation via fourth-order Runge-Kutta method, it is necessary to convert the two dimensionless second-order ordinary differential equations Eq. (11) into four dimensionless first-order ordinary differential equations.

NUMERICAL RESULTS

This section displays the numerical results obtained for free and damped forced vibrations and under different temperature configurations. The free vibration analysis identifies the equilibrium points. For the damped harmonically forced vibration several behaviors patterns are investigated through bifurcation diagrams and *Poincaré* sections characterizing periodic and chaotic-like responses for selected dimensionless forcing amplitude. The **SMA** parameters for all the cases are presented in Tab. 1, while Tab. 2 shows the dimensionless parameters used for dynamical analysis, there are three different linear damping coefficient, two distinct forcing frequency and the forcing amplitude is varied from 0.1 to 0.18 with steps of $1x10^{-4}$.

Table 1 – SMA properties and parameters for Savi's and co-workers model.

E_A (GPa)	E_M (GPa)	α (MPa)	ε_R
54	42	260	0.0555
L (MPa)	L_0 (GPa)	L^A (MPa)	L_0^A (MPa)
0.15	41.5	0.63	185
η_M^L (MPa/s)	η_M^U (MPa/s)	η_A^L (MPa/s)	η_A^U (MPa/s)
10.35	27	10	27
T_M (K)	T_0 (K)	Θ_A (Mpa/K)	Θ_M (Mpa/K)
291.4	288.5	0.74	0.17

Table 2– Dynamical system parameters

ξ	δ	ϖ
10^{-1}; 10^{-3}; 10^{-6};	Varying parameter	0.1; 2

The Fig. 2 displays the free vibration response for all three **SMA** elements subjected to a low-temperature ($\theta = 0.99$) and high-temperature ($\theta = 1.28$) conditions, in order to identify different equilibrium points. Two situations investigated regarding low-temperature condition the mass#*1* stabilizes in two different positions associated with both compressive detwinned martensite (Fig. 2a) and tractive detwinned martensite (Fig. 2b), according to the blue trajectories displayed on state subspaces U x U'. In both cases, mass#*2* stabilizes in a position associated with twinned martensite. The third case correspond to the high-temperature condition with both mass#*1* and mass#*2* resting at undeformed position associated to austenite (Fig. 2c), according to the red and dark yellow trajectories displayed on state subspaces U x U'. In this case all elements stabilize in a position associated with austenite.

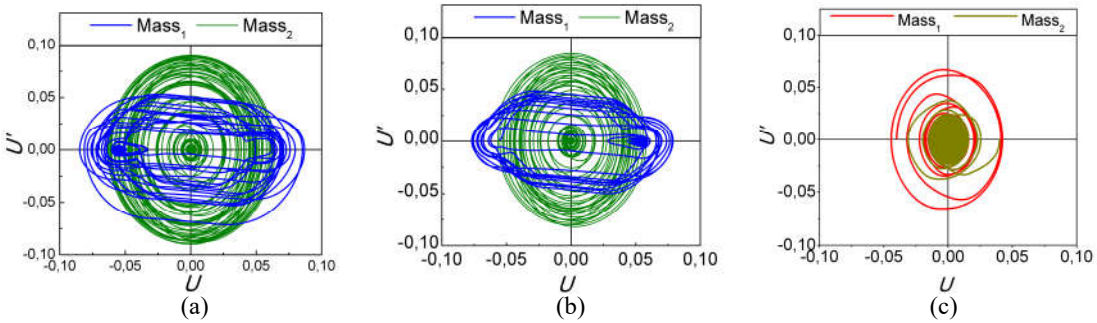

Figure 2 – Free vibration response for different initial conditions.

(a): $\left(U_{0_1} = -0.07; U_{0_2} = 0.05\right)$; **(b):** $\left(U_{0_1} = 0.07; U_{0_2} = 0.06\right)$;**(c):** $\left(U_{0_1} = 0.04; U_{0_2} = -0.04\right)$;

In Fig. 2a, mass#*1* stabilizes in a negative displacement position associated with compressive detwinned martensite for the element#1 which leads the element#2 to tractive detwinned martensite while the element#3 remains at twinned martensite, consequently, the mass#*2* stabilizes in a neutral position ($U = 0$) such that, after stabilization, the first **SMA** element is compressed, the second **SMA** element is stretched and the third ends up undeformed. Analogously, in Fig. 2b, mass#*1* stabilizes in a position associated with tractive detwinned martensite and mass mass#*2* stabilizes in a neutral position ($U = 0$) such that, the **SMA** element#1 is stretched and stable at tractive detwinned martensite, the **SMA** element#2 is compressed and converged to compressive detwinned martensite and the third element ends up

undeformed remaining at twinned martensite. The Fig. 3c both masses stabilize at neutral position ($U=0$) and all three elements remaining austenite.

Figure 3 exhibit the bifurcation diagrams of varying the forcing amplitude by the dimensionless displacement of both masses (U_1 and U_2) considering low-temperature (**LT**) and high-temperature (**HT**) conditions and, besides that, the dimensionless linear damping (ξ) and the dimensionless forcing frequency (ϖ) are switched. At first glance it is reasonable to assert, the behavior of the masses gain complexity as the damping become lower, another assertive related to the linear damping, for high damping (fig. 3a and fig. 3d) the dynamical behavior is a periodic of 1-period for both temperature conditions. At high temperature and high frequency ($\varpi=2$) (fig. 3d, fig. 3e and fig. 3f) displayed by the red and dark yellow line, the behavior is purely periodic of 1-period with very similar amplitudes of displacement for all the cases. Analyzing low temperature and high frequency, displayed by the same figures than before, but now blue and green lines, it is possible to see dynamic jump at the figure 3d, the other two diagrams (fig. 3e and fig. 3f) presents a very rich dynamical behavior with some periodic windows, cascading toward chaotic-like. The low frequency ($\varpi=0.1$) diagrams (fig. 3b and fig. 3c) exhibit a dynamical richness for both temperature conditions. Three forcing amplitude are selected, δ=0.1040, δ=0.14 and δ=0.1665 and for all these points of interest a *Poincaré* sections are performed to analyze the dynamical behavior.

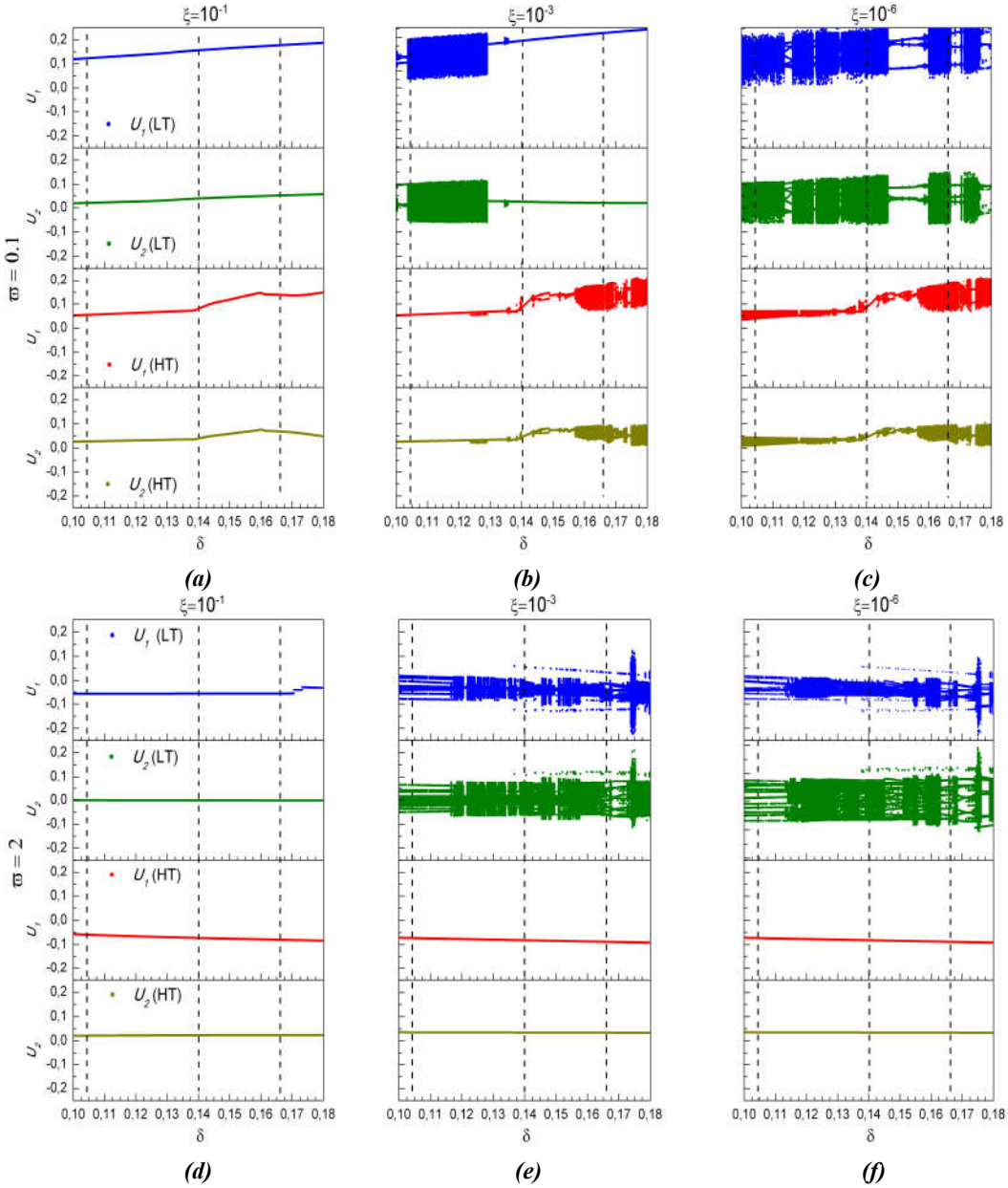

Figure 3 – Bifurcation diagrams for the forcing amplitude considering three distinct linear damping coefficients and two forcing frequencies; (a): $\left(\xi=10^{-1};\varpi=10^{-1}\right)$; (b): $\left(\xi=10^{-3};\varpi=10^{-1}\right)$;(c): $\left(\xi=10^{-6};\varpi=10^{-1}\right)$; (d): $\left(\xi=10^{-1};\varpi=2\right)$; (e): $\left(\xi=10^{-3};\varpi=2\right)$;(f): $\left(\xi=10^{-6};\varpi=2\right)$;

The figure 4 displays all *Poincaré* sections for a forcing amplitude δ=0.1040. At low temperature and low forcing frequency presented by fig. 4a, fig 4b and fig. 4c all cases are periodic, but the interesting point is that a periodic window is formed here, the orbit gain complexity and a 1-period become a 3-period which converts in a periodic of 5-period for both masses. About the high temperature condition considering the same frequency, it is worth to point the chaotic-like behavior (fig. 4c) despite of the 1-period for $\xi=10^{-3}$. and $\xi=10^{-1}$. The high frequency cases subject to low temperature condition presents many dynamical jumps, but the behavior stands periodic for a forcing amplitude lower than δ=0.11, at least, considering the beginning at δ=0.10. It is important highlighting, both masses present the same period quantity when the case is periodic.

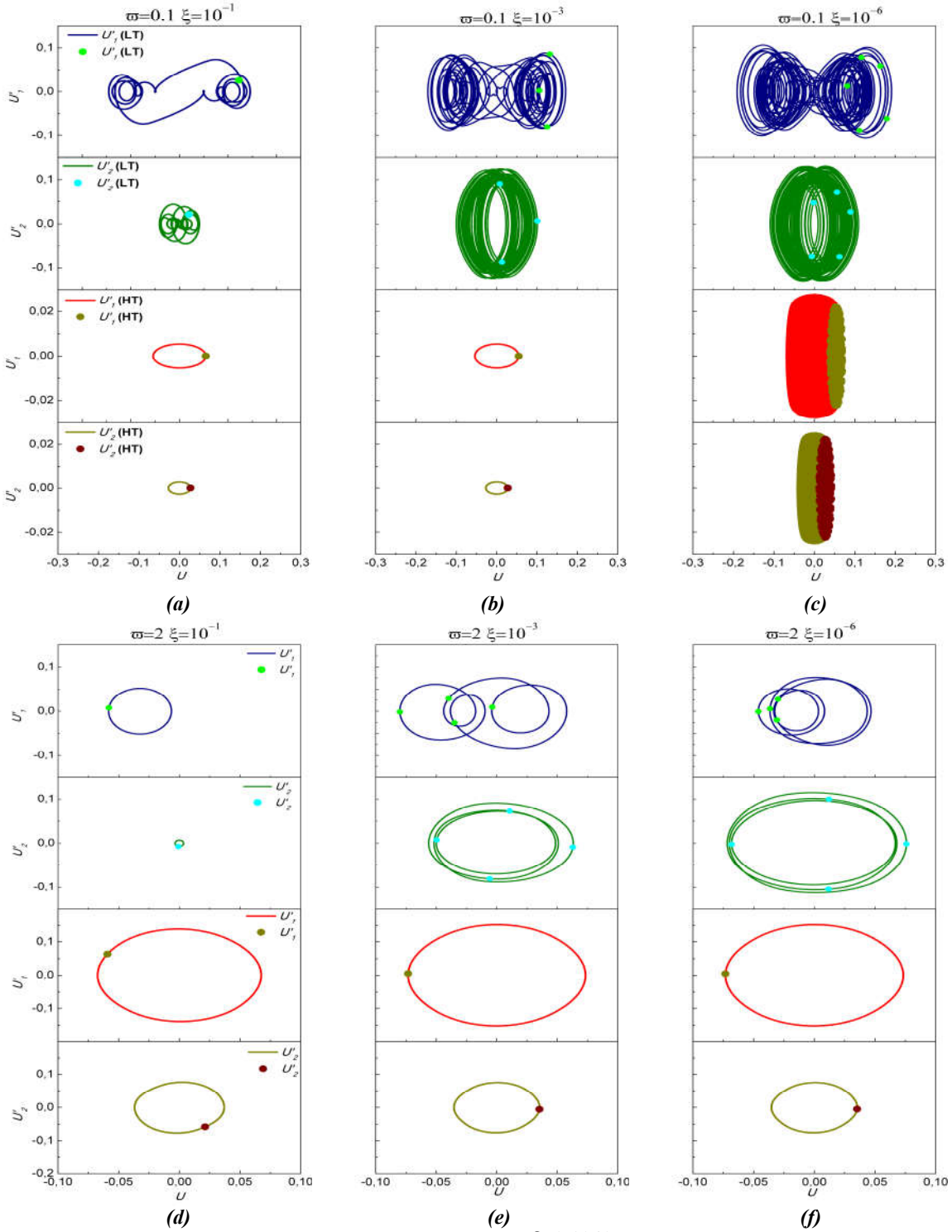

Figure 4 – *Poincaré* sections for a specific forcing amplitude (δ=0.1040), and different forcing frequency and damping. (a): $\left(\xi=10^{-1};\varpi=10^{-1}\right)$; (b): $\left(\xi=10^{-3};\varpi=10^{-1}\right)$;(c): $\left(\xi=10^{-6};\varpi=10^{-1}\right)$; (d): $\left(\xi=10^{-1};\varpi=2\right)$; (e): $\left(\xi=10^{-3};\varpi=2\right)$;(f): $\left(\xi=10^{-6};\varpi=2\right)$;

The *Poincaré* sections taken at δ=0.14 are showed below by the figure 5. For low temperature and forcing frequency equal to $\varpi=0.1$ (fig. 5a, fig. 5b and fig. 5c) the system's behavior change from periodic to chaotic-like, while the high temperature the periodicity stays the same from $\xi=10^{-1}$. and $\xi=10^{-3}$ but they have different state-space. The figure 5e presents for low temperature condition a high-period oscillation.

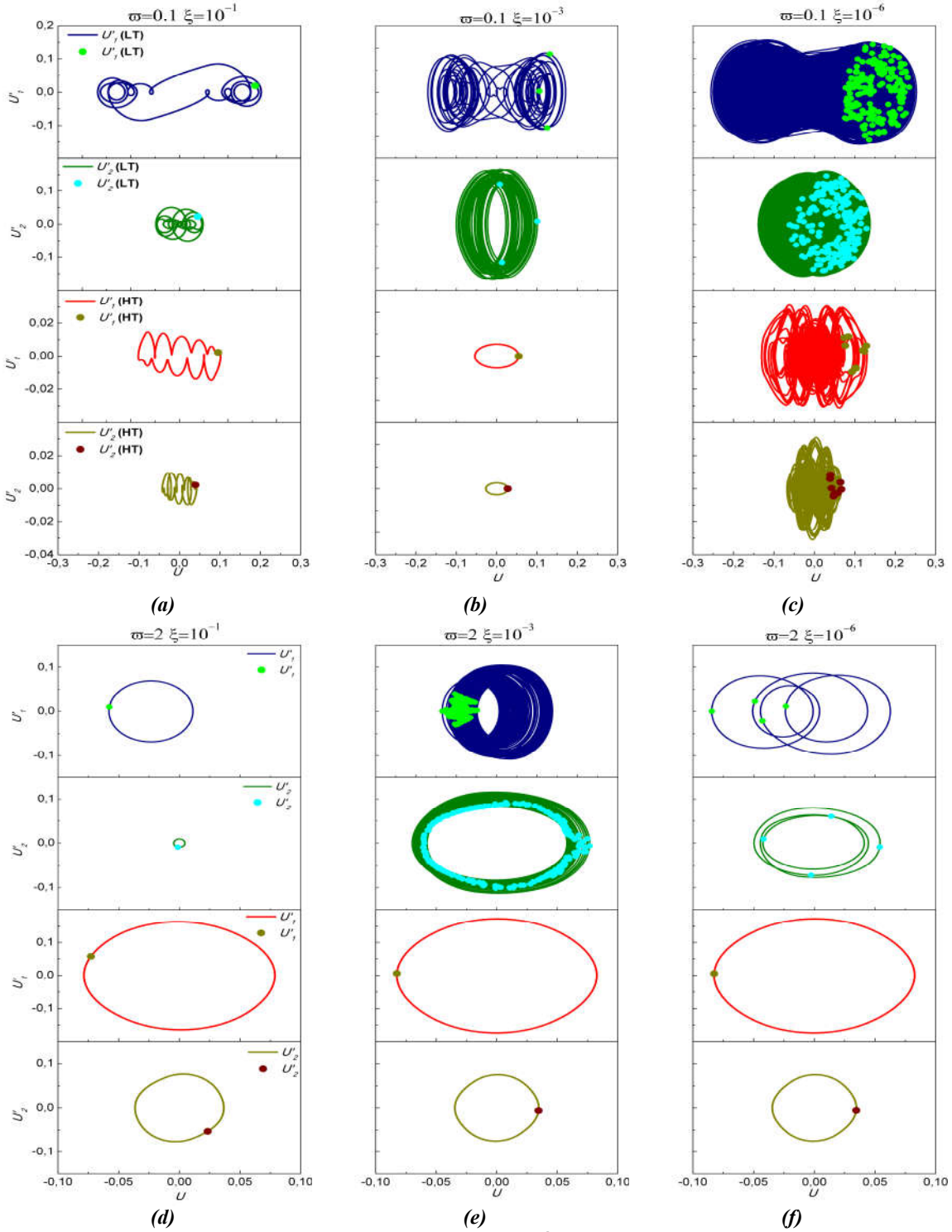

Figure 5 – *Poincaré* sections for a specific forcing amplitude (δ=0.14), and different forcing frequency and damping. (a): $\left(\xi=10^{-1};\varpi=10^{-1}\right)$; (b): $\left(\xi=10^{-3};\varpi=10^{-1}\right)$;(c): $\left(\xi=10^{-6};\varpi=10^{-1}\right)$; (d): $\left(\xi=10^{-1};\varpi=2\right)$; (e): $\left(\xi=10^{-3};\varpi=2\right)$;(f): $\left(\xi=10^{-6};\varpi=2\right)$.

The last *Poincaré* sections were taken at δ=0.1665 as per figure 6. This time for a forcing frequency equal to $\varpi=0.1$ (fig. 6a, fig. 6b and fig. 6c) the system's behavior evolve from periodic of 1-period to chaotic-like in both temperature conditions, while for a for a forcing frequency equal to $\varpi=2$ (fig. 6d, fig. 6e and fig. 6f) for low temperature condition,

the periodicity increases from 1-period for $\xi=10^{-1}$ to 4-period for $\xi=10^{-3}$, for both masses, however at $\xi=10^{-6}$ the mass#*1* is 21-period of periodic behavior while the mass#*2* is 22-period of periodic behavior.

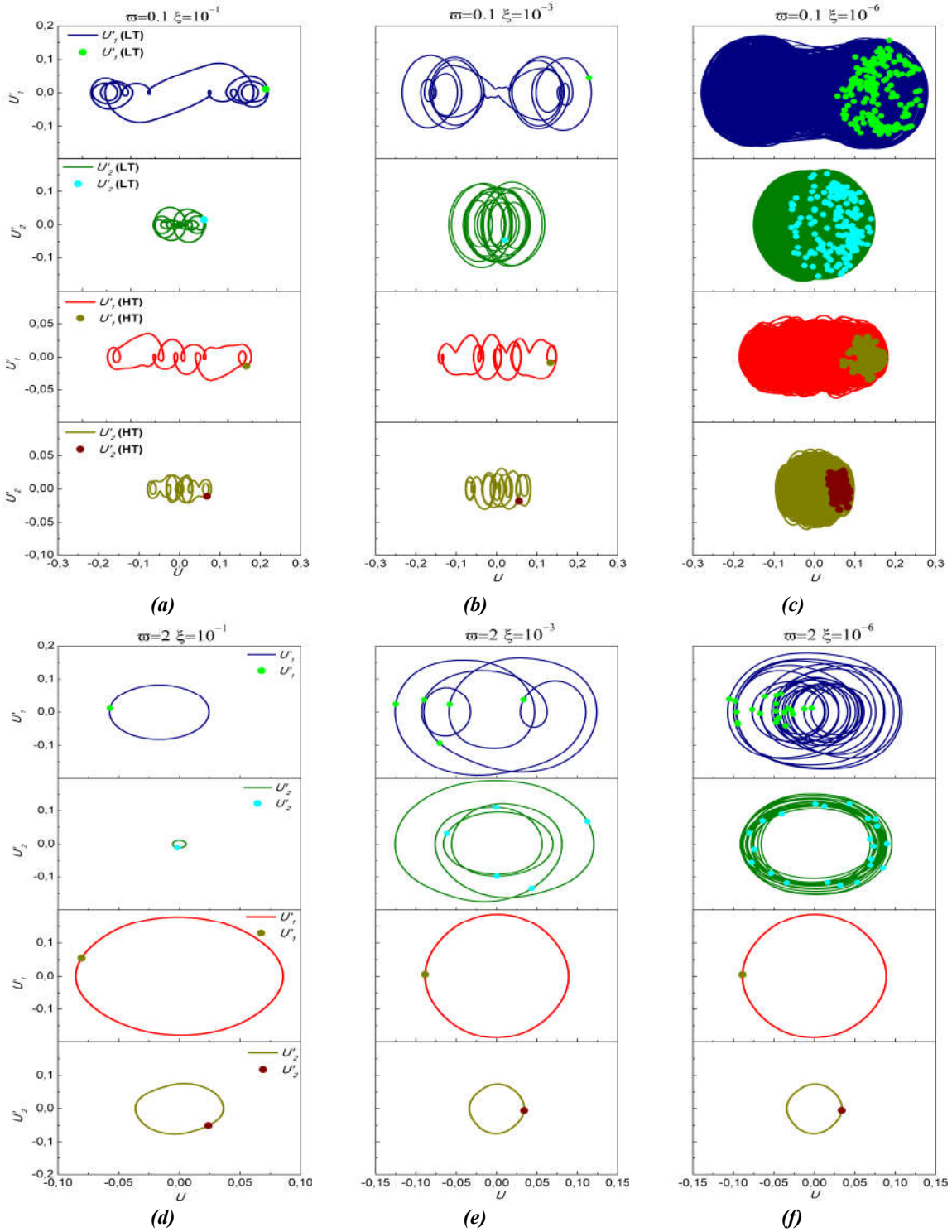

Figure 6 – *Poincaré* maps for an specific forcing amplitude (δ=0.1665), and different forcing frequency and linear damping. (a): $\left(\xi=10^{-1};\varpi=10^{-1}\right)$; (b): $\left(\xi=10^{-3};\varpi=10^{-1}\right)$;(c): $\left(\xi=10^{-6};\varpi=10^{-1}\right)$; (d): $\left(\xi=10^{-1};\varpi=2\right)$; (e): $\left(\xi=10^{-3};\varpi=2\right)$;(f): $\left(\xi=10^{-6};\varpi=2\right)$.

CONCLUDING REMARKS

This paper addresses the nonlinear analysis of a two-degree of freedom oscillator, considering three SMA restoring elements described by an internal constraints model. With respect to the numerical results, firstly, for free undamped vibration, the equilibrium points are identified at different temperatures. The investigation of the dynamical behavior for an harmonically forced case is conducted based on the variation of the forcing amplitude. The solutions are illustrated through trajectories on state spaces and Poincare sections.

ACKNOWLEDGMENTS

This study was financed in part by the Coordenação de Aperfeiçoamento de Pessoal de Nível Superior - Brasil (CAPES) Finance Code 001.

REFERENCES

Ricardo Alexandre Amar de Aguiar, Waldyr Cardoso de Castro Leão Neto, Marcelo Amorim Savi, Pedro Manuel Calas Lopes Pacheco, 2013, "Shape Memory Alloy Helical Springs Performance: Modeling and Experimental Analysis", Material Science Forum; Vol. 758; pp. 147-156.

Bernardini, D. & Rega, G.; 2005; "Thermomechanical Modelling, Non-linear Dynamics and Chaos in Shape Memory Oscilators"; Mathematical and Computer Modelling of Dynamical Systems; Vol. 11; N. 3; pp. 291–314.

Brinson, L.C., 1993, "One Dimensional Constitutive Behavior of Shape Memory Alloys: themomechanical derivation with non-constant material functions and redefined martensite internal variable", Journal of Intelligent Material Systems and Structures, Vol. 4, pp. 229–242.

Enemark, S., Savi, M.A. & Santos, I.F; 2014; "Nonlinear Dynamics of a Pseudoelastic Shape Memory Alloy System – Theory and Experiment"; Smart Material and Structures; Vol. 23; Article ID 085018; 17 pp.

Falk, F.; 1980; "Model Free-energy, Mechanics and Thermodynamics of Shape Memory Alloys"; ACTA Metallurgica; Vol. 28; pp. 1773–1780.

Fremond, M.; 1987; "Matériaux à Mémoire de Forme"; C.R. Acad. Sc. Paris; Vol. II, N. 7; pp. 239–244.

Gaikwad, S.R & Pandey, A.K.; 2018; "Nonlinear Analysis of Shape Memory Devices with Duffing and Quadratic Oscillators"; Journal of Computational and Nonlinear Dynamics; Vol. 13; 8 pp.

Machado, L.G., Savi, M.A. & Pacheco, P.M.C.L.; 2003; "Nonlinear Dynamics and Chaos in Coupled Shape Memory Oscillators"; International Journal of Solids and Structures; Vol. 40; N. 19; pp. 5139–5156.

Paiva, A., Savi, M.A., Braga, A.M.B., Pacheco, P.M.C.L.; 2005; "A Constitutive Model for Shape Memory Alloys Considering Tensile-compressive Asymmetry and Plasticity. International Journal of Solids and Structures; Vol. 42; N. 11-12; pp. 3439–3457.

Rajagopal, K., Karthikeyan, A., Duraisamy, P. & Weldegiorgis, R.; 2018; "Bifurcation and Chaos in Integer and Fractional Order Two-Degree-of-Freedom Shape Memory Alloy Oscillators"; Complexity; Vol. 2018; Article ID 8365845; 9 pp.

Rodrigues, G.V., Mendonça, G.L.T., Paiva, A. & Savi, M.A.; 2017; "Dynamical Stability Analysis of a 2-DOF SMA Oscillator"; Proceedings of XVII International Symposium on Dynamic Problems of Mechanics – DINAME 2017.

Rusineka, R., Warminski, J., Szymanski, M., Kecika, K. & Kozik, K.; 2017; "Dynamics of the Middle Ear Ossicles with an SMA Prosthesis"; International Journal of Mechanical Sciences; Vol. 127; pp. 163–175.

Savi, M.A., De Paula, A.S. & Lagoudas, D.C.; 2011; "Numerical Investigation of an Adaptive Vibration Absorber Using Shape Memory Alloys" Journal of Intelligent Material Systems and Structures; Vol. 22; pp. 67–80.

Savi, M.A., Sa, M.A.N., Paiva A. & Pacheco, P.M.C.L.; 2008; "Tensile-compressive Asymmetry Influence on Shape Memory Alloy System Dynamics"; Chaos, Solitons and Fractals; Vol. 36; pp. 828–842.

Savi, M.A.; 2015; "Nonlinear Dynamics and Chaos in Shape Memory Alloy Systems"; International Journal of Non-Linear Mechanics; Vol. 70; pp. 2–19.

Silva, L.C., Savi, M.A. & Paiva, A.; 2013; "Nonlinear Dynamics of a Rotordynamic Nonsmooth Shape Memory Alloy System"; Journal of Sound and Vibration; Vol. 332; pp. 608–621.

Sitnikova, E., Pavlovskaia, E., Ing, J. & Wiercigroch, M.; 2012; "Suppressing Nonlinear Resonances in an Impact Oscillator Using SMAs"; Smart Material and Structures; Vol. 21; Article ID 075028; 16pp.

Wang, L. & Melnik, R.V.N.; 2012; "Nonlinear Dynamics of Shape Memory Alloy Oscillators in Tuning Structural Vibration Frequencies"; Mechatronics; Vol. 22; pp. 1085–1096.

RESPONSIBILITY NOTICE

The authors are the only responsible for the printed material included in this paper. "This study was financed in part by the Coordenação de Aperfeiçoamento de Pessoal de Nível Superior - Brasil (CAPES) Finance Code 001"